

Quasiclassical trajectory calculations of collisional energy transfer in propane systems: Multiple direct-encounter hard-sphere model

Apichart Linhananta† and Kieran F. Lim*‡

Centre for Chiral and Molecular Technologies, School of Biological and Chemical Sciences, Deakin University, Geelong, Victoria, 3217, Australia. E-mail: lim@deakin.edu.au

Received 8th October 2001, Accepted 27th November 2001

First published as an Advance Article on the web 16th January 2002

Quasiclassical trajectory calculations of collisional energy transfer from highly vibrationally excited propane + rare gas systems are reported. This work extends our hard-sphere model (A. Linhananta and K. F. Lim, *Phys. Chem. Chem. Phys.*, 2000, **2**, 1385) to examine the variation of the internal energy during collisions with a rare bath gas. This was accomplished by recording the vibrational and rotational energy of propane after each atom–atom encounter during trajectory simulations of propane + rare gas systems. This provides detailed information of the energy flow during a collision. It was found that collisions with small number of encounters transfer energy efficiently, whereas those with many encounters do not. Detailed analyses reveal that the former collisions arise from trajectories with high initial impact parameter, whereas the latter have small initial impact parameter. The reason behind this is the dependence of collision energy transfer (CET) of large polyatomic molecules on their shape. This is connected to the well-known role of rotational energy transfer (RET) as a gateway for CET.

I. Introduction

It is well established that collision energy transfer (CET) plays a vital role in gas phase kinetics.^{1,2} Recently, we have performed quasiclassical trajectory (QCT) calculations on ethane + rare gas³ and propane + rare gas⁴ systems. Since ethane and propane are combustion fuels, these studies have commercial as well as scientific relevance. These calculations are part of a general study on combustion-model and atmospheric-model systems. The main goal is to unravel the CET mechanism of common fuels such as alkanes, branched-alkanes and their halogenated analogues. Most CET studies of large polyatomics have been on aromatic compounds chosen for their amenable spectroscopic properties.^{2,5}

Ethane is a major (~9%) component of natural gas. Propane is the primary constituent of liquefied petroleum gas (LPG). Both of these fuels present a new challenge in CET studies because they have methyl torsional rotors. Larger alkane fuels such as butane (lighter fluid) and octane (prototypical automotive fuel) have, in addition, backbone torsional conformations. For the theoretician, simulations of alkane systems would require the development of algorithms that correctly sample the conformational degrees of freedom. Our calculations of ethane³ and propane⁴ systems found that, even for smaller alkanes, torsional vibrational modes have a significant role in the CET mechanism. The initial collision between alkane + bath gas heats up the external rotor. In subsequent collisions, the coupling between the internal and external rotors results in facile CET *via* V,torsion → torsion,R,T. This is in accord with other theoretical work which predicted that rotational energy transfer (RET) is a gateway for collisional energy transfer.^{6,7} This is very sig-

nificant since rotational excitations would accelerate the rate of dissociation of hydrocarbon fuels into radical species conducive to combustion. Indeed several researchers have remarked that such reactions must be modelled by a 2-dimensional master equation in the variables J and E .^{1,8,9} A key point is that in a combustion reaction, molecules are highly vibrationally excited and due to strong rovibrational couplings it is not possible to determine the rotational distribution.

Experimental determinations of CET in alkane systems have inferred CET quantities by use of a one-dimensional master equation analysis.¹⁰ These earlier results do not have information about the interdependence of rotational and vibrational energy transfer. Hence theoretical calculations are the only means of investigating the interdependence of rotational and vibrational energy transfer in CET.

To date, our understanding of the CET mechanism in polyatomic systems is incomplete. Thus simple tractable models are appropriate since they illuminate aspects which remain hidden under more realistic classical or semiclassical models. Nordholm and coworkers have developed a number of statistical models for CET,¹¹ which can be considered to be loosely related to the sequential direct encounter model of Dashevskaya *et al.*¹² These models, either implicitly or explicitly, classified collisions into two main groups: (1) direct collisions which comprise a single atom–atom encounter; (2) “chattering collisions” in which there are sequences of multiple encounters. Our QCT simulations of argon + toluene collisions indicate that about 90% of collisions can be classified into these two categories.¹³ For direct collisions, the energy transfer is dependent on the repulsive part of the intermolecular interaction. Chattering collisions occur under near-adiabatic conditions and the energy transfer process is near-ergodic. Hence, Dashevskaya *et al.* analysed the energy flow from hot polyatomics to the bath gas by diffusion equations,¹² similar to the approach of our biased random walk model.^{14,15}

† Current address: Department of Physiology/Biophysics, SUNY at Buffalo, Buffalo, NY 14214, USA.

‡ 林百君 (Lim Pak Kwan).

The impetus for the development of approximate models^{11,12,14,15} arises because quantum and semiclassical or classical dynamics become impractical for large systems. Hence, we investigated the possibility of using hard-sphere (HS) collision dynamics in a preceding paper.⁴ This previous work involved qualitative and quantitative comparison of the HS model with full quasiclassical trajectory calculations using two intermolecular potential models (atom pairwise-additive Lennard-Jones and atom pairwise-additive Buckingham-exponential models).⁴ We found that although the HS model resulted in CET and RET values that are too high, the model produced correct qualitative behaviours.⁴ A key point is that the HS model has no intermolecular interaction until the point of impact (or “direct encounter”). Hence the equations of motion are integrated for a comparatively short period resulting in substantially reduced computation. This will be crucial for theoretical investigations of larger flexible alkanes, in which the number of interatomic interactions scales as the square of the number of atoms (or worse), the increased collider masses result in longer trajectories, and there are larger phase spaces to sample.

This paper seeks to elucidate the connections between RET and CET, which play key roles in combustion processes. This is done by employing a multiple direct-encounter HS model for collisions between propane and a rare gas. The loss of quantitative prediction is compensated by the increased computational efficiency, allowing prediction of detailed qualitative trends. By recording the internal energy of propane after each atom–atom encounter, the detailed mechanism behind the energy flow during a collision is investigated. Our calculations are able to determine the relative CET efficiencies between direct collisions (low encounter number) and chattering collisions (high encounter number). The temporal evolution of RET and CET during collisions is examined. Finally, the diffusive-like temporal behaviour of the internal and rotational energy transfer distributions during a collision is reported.

II. Quasiclassical trajectory calculations

A. Potential energy surface

A simple harmonic valence force field, as used previously,⁴ was employed.

$$V_{\text{intra}} = \sum_i V_{\text{stretch},i} + \sum_i V_{\text{bend},i} + \sum_i V_{\text{torsion},i}$$

These terms have been defined previously,^{3,4,16–18} with harmonic stretch and bend force constants^{4,19}

$$\begin{aligned} k_{\text{str,CC}} &= 4.705 \times 10^2 \text{ J m}^{-2}, \\ k_{\text{str,CH}} &= 4.702 \times 10^2 \text{ J m}^{-2}, \\ k_{\text{bend,CCH}} &= 6.67 \times 10^{-17} \text{ J rad}^{-1}, \\ k_{\text{bend,HCH}} &= 5.61 \times 10^{-17} \text{ J rad}^{-1}. \end{aligned}$$

The torsional barrier is taken to be the experimentally observed²⁰ value of $V_0 = 13.8 \text{ kJ mol}^{-1}$. Each carbon centre was assumed to have perfect tetrahedral equilibrium geometry with C–C and C–H bond lengths of 0.1543 nm and 0.1093 nm, respectively.

The intermolecular potential was a pairwise-additive hard-sphere potential with atom–atom terms V_{ij} given by

$$\begin{aligned} V_{ij} &= \infty, & r_{ij} &\leq r_{ij}^{\text{vdW}}, \\ &= 0, & r_{ij} &> r_{ij}^{\text{vdW}}, \end{aligned} \quad (1)$$

($i = \text{C,H}$; $j = \text{rare gas}$), where r is the atom–atom center-of-mass separation and r_{ij}^{vdW} is the van der Waals radius²¹ (see Table 1).

Table 1 Intermolecular van der Waals radii ($r_{ij}^{\text{vdW}}/\text{nm}$)

Collider bath gas	Substrate atom	
	H	C
He	0.325	0.345
Ne	0.305	0.325
Ar	0.335	0.355

B. Computational details

Trajectory calculations were performed using program MARINER,¹⁷ which is a customised version of VENUS96.¹⁸ The selection of initial conditions and general methodology are standard options in program MARINER/VENUS96.^{17,18,22} The HS interaction potential was incorporated by us⁴ into the program MARINER. The initial impact energy E_{trans} was chosen from a 300 K thermal distribution. The initial impact parameter b was chosen with importance sampling^{17,18,22–24} from the distribution:

$$(fb) db = \frac{db}{b_m}, \quad 0 \text{ nm} \leq b \leq 0.7 \text{ nm}$$

Importance sampling was chosen over Monte Carlo sampling since it is biased to low impact parameter trajectories, which transfer more energy and contribute more significantly to average CET.

For the HS model, there is no intermolecular interaction until the point of impact (*i.e.*, the first atom–atom encounter), at which point the trajectory is started. Up to, and including, the point of impact, the propane molecule is described by a (near-) microcanonical ensemble. The initial rotational angular momentum of propane was chosen from a thermal distribution at 300 K. The initial vibrational phases and displacements were chosen from microcanonical ensembles at $E' = 41\,000$, 30 000 or 15 000 cm^{-1} , where E' is the rovibrational energy above the zero-point energy. These initial conditions are appropriate for comparison with the first few collisions in time-resolved infrared fluorescence, ultraviolet absorption and time-resolved optoacoustic experiments used for experimental study of alkanes and aromatic systems.^{2,25–27} Note that these experiments measure the CET values of a cascade of collisions. The rovibrational energy distribution of subsequent collisions will not be microcanonical, but the CET behaviour of subsequent collisions can be inferred^{3,4,6,28} from microcanonical values.

Computationally, the selection of initial conditions was implemented by placing the propane molecule and rare gas atom at an arbitrary center-of-mass separation, and choosing the initial positions, momenta, relative orientation, *etc.*, as described above. The centre-of-mass separation was then chosen to be the distance, which was defined by the point of initial contact.²⁹ (Initial conditions, chosen as described here, which do not result in collision are still included in the statistics as non-collisional or elastic events: see discussion below.)

The actual trajectories were propagated by a predictor–integrator method:

(a) For interatomic distances $r_{ij} > r_{ij}^{\text{vdW}}$ (eqn. (1)), there is no difference between the HS potential and having no intermolecular potential. Hence the trajectory was propagated normally, but in the absence of an intermolecular potential, using a Adams–Moulton predictor–corrector algorithm, which has been initiated by a Runge–Kutta algorithm.^{17,18,22} This constituted the predictor step, using a fixed time step of 0.085 fs for $E' = 15\,000$ and 30 000 cm^{-1} , and 0.075 fs for $E' = 41\,000 \text{ cm}^{-1}$. These integration time steps were sufficient to conserve total energy to within 0.5 cm^{-1} ;

(b) At each time step, the trajectory was interrogated to determine whether the predictor step would move the

trajectory into the classically forbidden region $r_{ij} < r_{ij}^{\text{vdW}}$ (eqn. (1)). If the trajectory remained in the classically allowed region, the predicted atomic positions and momenta were accepted and another time-step predicted using (a). If, however, the trajectory had entered the classically forbidden region, then the predicted positions and momenta were rejected, and the time-step altered to one which placed the atomic positions and momenta at the boundary of the forbidden region $r_{ij} = r_{ij}^{\text{vdW}}$: this variable time-step integrator step finds the instant at which the vdW hard sphere of an atom in propane is impacting (touching) the rare gas vdW hard sphere. At this point, the impulsive momentum transfer was calculated.²⁹ The trajectory is then continued using the predictor step (a).

Variants of this predictor-integrator method have been used for simulations of HS liquids,²⁹ for constrained-dynamics, which preserved the quantum zero-point energy in pseudo-classical simulations,³⁰ for hard-shell dynamics^{29,31} and the use of molecular shapes in pharmaceutical drug design and related fields.³²

This process was repeated until another encounter occurred or until the distance between the monatomic collider and the closest hydrogen exceeded a critical value, which was taken to be 0.4 nm, at which point the trajectory was terminated. For this work, Program MARINER¹⁷ was modified so that the coordinates, momenta and energy of the systems are recorded after each encounter. This enables the temporal behaviour of the energy flow to be monitored during a collision.

Sets of 70 000–200 000 trajectories were calculated for propane + rare gas (He, Ne, Ar) collisions. Although overall CET and RET quantities can be established by smaller numbers of trajectories, these large sets were required for analysis of longer-lived collisions, which are infrequent events. The calculations were performed on a DEC Alpha 3000/300LX workstation and a SGI Power Challenge Supercomputer.

The advantage in computer time of the HS approach is enormous. For example, based on our previous calculations,^{3,4} we estimate that 100 000 propane + helium trajectories, employing a (full) pair-wise additive Lennard-Jones (LJ) potential, would require approximately 10^3 cpu hours for a vectorised program running on a supercomputer. In comparison, the HS model required only 30 cpu hours on a UNIX workstation.

C. Encounter number

An atom–atom encounter can be unambiguously defined as a hard-sphere impact between the bath gas atom and an atom on the substrate. Each atom–atom encounter corresponds to one occurrence of the Slater-theory-like³³ event $r_{ij} = r_{ij}^{\text{vdW}}$ (eqn. (1)). Most collisions consist of a sequence of encounters between the bath gas atom and one or more atoms on the substrate. A direct collision consists of a single atom–atom encounter. The overall collision duration is measured by the total number of atom–atom encounters, En . The time between encounters corresponds roughly to a CH stretching vibrational period.¹⁴ The progress of the collision is measured by counting the number of encounters, up to the maximum En .

Following the notation of references,^{14,34} $B(E, J, E', J', l)$ is defined as the distribution of polyatomic substrate energies and angular momenta (E, J) after l encounters, where the initial microcanonical distribution is a delta function:

$$B(E, J, E', J', l = 0) = \delta(E - E') \delta(J - J').$$

The probability of energy transfer $P(E, J, E', J')$ is the B distribution at the conclusion of the collision:

$$P(E, J, E', J') = B(E, J, E', J', l \rightarrow \infty).$$

Since the trajectories can be divided into subsets, each with a different total encounter number En , this last equation should be a weighted average of B distributions

$$P(E, J, E', J') = \frac{\sum_{En=1}^{\infty} N(En) B_{En}(E, J, E', J', l \rightarrow En)}{\sum_{En=1}^{\infty} N(En)} \quad (2)$$

where $N(En)$ is the number of trajectories with total encounter number En , and B_{En} is the time-dependent B -distribution for the subset of trajectories of total encounter number En .

D. Data analysis

Trajectory data were analysed by a bootstrap algorithm³⁵ in Program PEERAN.^{23,36} For importance sampling, trajectory averages defined by $\langle \Delta E^n \rangle_{\text{traj}}$

$$\langle \Delta E^n \rangle_{\text{traj}} = \frac{1}{N} \sum_{i=1}^N \frac{2b_i}{b_m} (\Delta E_i)^n, \quad (3)$$

are related to experimentally obtained quantities $\langle \Delta E^n \rangle$ by the ratio of the collision cross sections

$$\langle \Delta E^n \rangle = \frac{\pi b_m^2}{\pi \sigma_{\text{LJ}}^2 \Omega^{(2,2)*}} \langle \Delta E^n \rangle_{\text{traj}}, \quad (4)$$

where the product $\pi \sigma_{\text{LJ}}^2 \Omega^{(2,2)*}$ is the LJ collision cross-section³⁷ and b_m is the maximum impact parameter in the trajectory simulation. In eqn. (4), σ_{LJ} is the LJ collision diameter, found from the individual LJ collision radii for propane and the appropriate rare gas atom by the Lorentz–Berthelot combining rules,³⁸ while $\Omega^{(2,2)*}$ is the reduced collision integral appropriate to the coefficient of viscosity and thermal conductivity.³⁷ The choice of the product $\pi \sigma_{\text{LJ}}^2 \Omega^{(2,2)*}$ as the reference collision cross-section is discussed below. This normalisation, removes the ambiguity related to the elastic scattering.³⁴ The LJ parameters were obtained from ref. 27. Program COLRATE³⁹ was used to find the LJ collision cross-sections, $\pi \sigma_{\text{LJ}}^2 \Omega^{(2,2)*}$, which are listed in Table 2. These correspond to LJ collision frequencies $Z_{\text{LJ, coll}} = 523.29 \times 10^{-18} \text{ m}^3 \text{ s}^{-1}$, $328.58 \times 10^{-18} \text{ m}^3 \text{ s}^{-1}$ and $382.37 \times 10^{-18} \text{ m}^3 \text{ s}^{-1}$, at 300 K for propane + He, propane + Ne and propane + Ar, respectively.

Table 2 Collision cross-sections for propane + collider collisions

Collider bath gas	Propane excitation energy, E'		
	15 000 cm^{-1}	30 000 cm^{-1}	41 000 cm^{-1}
Trajectory cross-section ($\sigma_{\text{traj}}/\text{nm}^2$): eqn. (6). All trajectories used $b_m = 0.7 \text{ nm}$: see ref. 4.			
He	1.540	1.540	1.540
Ne	1.540	1.540	1.540
Ar	1.540	1.540	1.540
Inelastic collision cross-section (σ/nm^2): eqn. (7)			
He	1.050	1.053	1.055
Ne	1.007	1.010	1.011
Ar	1.073	1.076	1.077
LJ collision cross-section ($\pi \sigma_{\text{LJ}}^2 \Omega^{(2,2)*}/\text{nm}^2$): ref. 27, 37, 39			
He	0.3976	0.3976	0.3976
Ne	0.4834	0.4834	0.4834
Ar	0.6945	0.6945	0.6945

Trajectory data are weighted by the factor b_i/b_m (in a similar fashion to eqn. (3),) to obtain the distribution functions, B , and related quantities.

The change in rotational energy, $\langle \Delta E_R \rangle$, was calculated using the approximate rotational energy:⁴

$$E_R \approx \frac{J^2}{2 \sqrt[3]{I_{xx} I_{yy} I_{zz}}}, \quad (5)$$

where J is the magnitude of the rotational angular momentum and $I_{xx} = 1.11 \times 10^{-45} \text{ kg m}^2$, $I_{yy} = 9.7 \times 10^{-46} \text{ kg m}^2$ and $I_{zz} = 2.97 \times 10^{-46} \text{ kg m}^2$ are the equilibrium Cartesian moments of inertia.

III. Results and discussion

A. Collider mass and initial excitation energy

Table 2 shows the inelastic collision cross-sections, σ , obtained from trajectory simulations.

$$\sigma_{\text{traj}} = \pi b_m^2, \quad (6)$$

$$\sigma = \sigma_{\text{traj}} F, \quad (7)$$

where F is the fraction of trajectories with one or more atom-atom encounters. Note that there is some potential for confusion here as the literature uses the symbol σ for both various collision cross-sections (*e.g.* Table 2 and eqns. (6) and (7)) and for the LJ radius or diameter (*e.g.* eqn. (4)).

The circles in Fig. 1 show schematically where the centre of the incoming monatomic collider might impact on the propane molecule at varying impact parameters $b = 0.1\text{--}0.5 \text{ nm}$. (The actual location of the initial impact will depend on the relative orientations of the colliders.) It can be seen that *every* trajectory with $b > ca. 0.6 \text{ nm}$ will *not* result in a collision, regardless of the propane orientation: the opacity function (probability of an inelastic collision) is zero for large impact parameters.^{34,40} This cut-off between zero and non-zero opacity function defines the maximum impact parameter b_m , and the trajectory cross-section σ_{traj} (eqn. (6)). We have previously noted that σ_{traj} is much larger than the LJ cross-section $\pi \sigma_{\text{LJ}}^2 \Omega^{(2,2)*}$.^{16,34}

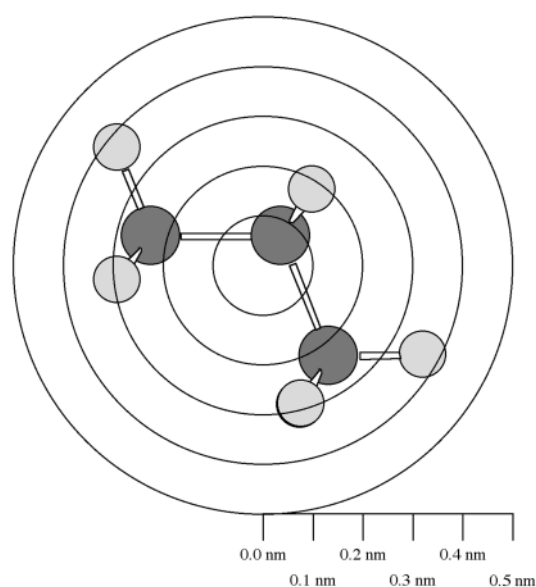


Fig. 1 Schematic diagram showing impact parameter, b , relative to propane. The carbon and hydrogen diameters are not the van der Waals radii, but are for illustrative purposes only. Circles are placed at 0.1 nm intervals and are centred on the propane centre-of-mass.

Subsequently, Lendvay and Schatz found that σ_{traj} is on average 3.1 times $\pi \sigma_{\text{LJ}}^2 \Omega^{(2,2)*}$ for a number of CS_2 , SF_6 , and SiF_4 systems:⁴⁰ the Table 2 results are consistent with these previous findings. Inspection of Fig. 1 indicates that *every* trajectory for $b < ca. 0.4 \text{ nm}$, results in a “head-on” collision: the opacity function is unity, while for $ca. 0.4 \text{ nm} < b < ca. 0.6 \text{ nm}$, *some* trajectories result in collision while other trajectories result in no collision, depending on the relative orientation and motions of the propane molecule and atomic collider: opacity function is decreasing over this intermediate impact parameter range. The conclusion is that the trajectory cross-section σ_{traj} includes many inelastic non-collisional events.³⁴

For this reason, the total elastic cross-section σ is defined by eqn. (7) and listed in Table 2. Most intermolecular potentials and model potentials have small non-zero contributions extending to very large intermolecular separations: “collisions” are ill-defined, and are dependent on the property or process being investigated. Since the HS model of this work (and related models) have intermolecular potentials with a very well-defined interaction cut-off distance (eqn. (1)), the collision events are well-defined. This is a further advantage of the HS model, which enables the gathering of unambiguous data to aid the development of approximate models for CET.

In contrast to trajectory studies, experimental studies observe rates, which are related to actual cross-sections.⁴¹ In CET studies, these are the energy transfer rates and elastic cross-sections, respectively.³⁴ However, the energy transfer rate is a product of the collision rate and the cross-section, but the factorisation of the rate into its constituent factors is not unique. Lawrance and Knight’s experimental study of CET between *p*-difluorobenzene (S_0) and a variety of collision partners, showed that the total elastic cross-section was equal to the LJ cross-section given as the denominator of eqn. (4).⁴² (There are a whole family of different LJ cross-sections, each defined by a different $\Omega^{(m,n)*}$ collision integral,³⁷ but the one most commonly used is the reduced collision integral denoted by the (2,2)* superscript.) There have also been theoretical discussions why the $\pi \sigma_{\text{LJ}}^2 \Omega^{(2,2)*}$ collision cross-section³⁷ should be the appropriate reference cross-section: for example, see ref. 8,43.

The trajectory cross-section σ_{traj} and inelastic collision cross-section σ depend on the van der Waals radii, and the shape of the substrate (propane): see Fig. 1. The observed trend ($\text{Ar} > \text{He} > \text{Ne}$: Table II) is due to the van der Waals radius of He being larger than Ne (see Table 1). A small increase is observed with the increase of the initial excitation energy, E' , of the propane substrate. This is related to the small increase in the vibrationally-averaged bond lengths with increasing excitation.

The discrepancy between the computed inelastic cross-sections and the LJ cross-section, which has some experimental justification,⁴² indicates the need for better intermolecular potential functions to be used in trajectory simulations, probably along the lines of the work of Collins and his co-workers.⁴⁴

Fig. 2 shows the distribution of collision durations, where collision duration is measured by the total encounter number, En , at $E' = 15\,000 \text{ cm}^{-1}$. The distribution includes only inelastic collision trajectories with at least one atom-atom encounter. For helium bath gas the distribution peaks at $En = 1$ and decreases rapidly thence. As the reduced mass increases, the collision partners have lower relative velocity, shifting the distribution to slightly higher En for Ne and Ar bath gases. Overall, most collisions tend to be short-lived and impulsive, consistent with our earlier QCT simulations of argon + toluene collisions.¹³ There is insufficient time for equilibration of energy between the different degrees of freedom.

Fig. 3 plots the distribution of collision durations (as measured by the encounter number, En) for an argon bath gas at $E' = 15\,000$, $30\,000$ and $41\,000 \text{ cm}^{-1}$. There is a slight shift to slightly shorter En as E' is increased. This can be seen as the

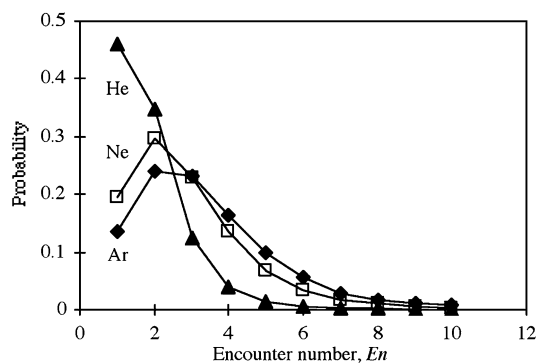


Fig. 2 Distribution of collision durations (measured by E_n) for propane + rare gas systems at $E' = 15000 \text{ cm}^{-1}$.

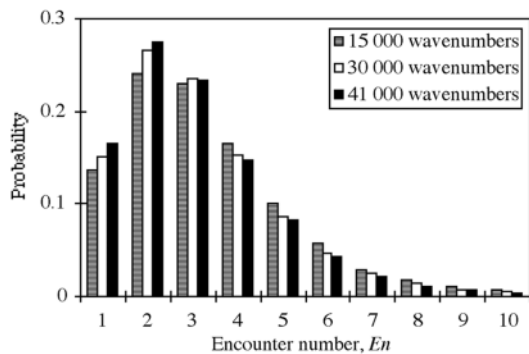


Fig. 3 Distribution of collision durations (measured by E_n) for propane + Ar systems.

distributions increase with E' for short E_n ($E_n = 1, 2$) but the distributions decrease with E' for longer E_n .

Fig. 4 shows the average total ($-\langle\Delta E\rangle$) and rotational ($\langle\Delta E_R\rangle$) energy transfer per collision as functions of E_n , as bath gas is varied. Note that these are energy transfer values for inelastic collisions at fixed E_n : eqns. (3)–(5) are applied to subsets of trajectories, where each subset has a different E_n value (cf. our earlier work¹³). The trends of $\text{He} > \text{Ne} > \text{Ar}$ for $-\langle\Delta E\rangle$ and $\text{Ne} > \text{Ar} > \text{He}$ for $\langle\Delta E_R\rangle$ are consistent with the

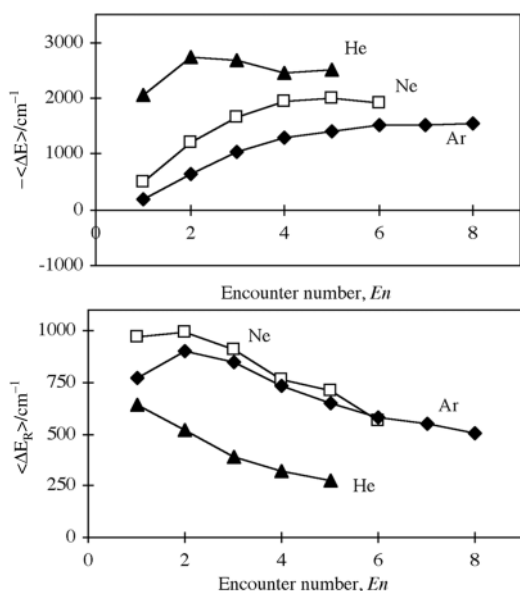


Fig. 4 $-\langle\Delta E\rangle$ and $\langle\Delta E_R\rangle$ for propane + rare gas systems at $E' = 15000 \text{ cm}^{-1}$. Each data point represents a different trajectory subset, where each subset has a different E_n value.

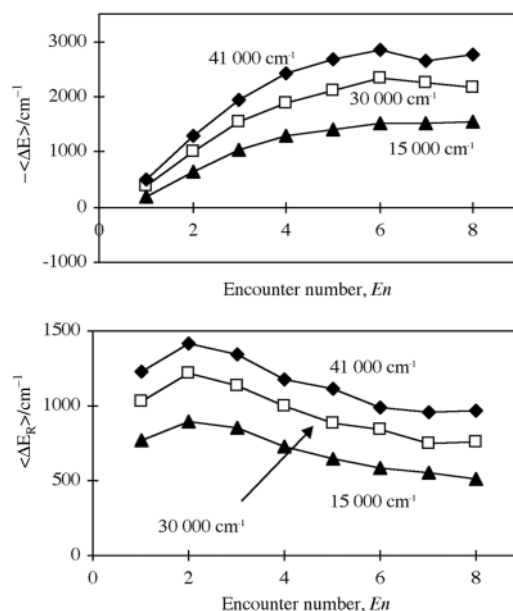


Fig. 5 $-\langle\Delta E\rangle$ and $\langle\Delta E_R\rangle$ for propane + Ar systems. Each data point represents a different trajectory subset, where each subset has a different E_n value.

total CET and RET values of ref. 4. In general, $-\langle\Delta E\rangle$ increases with E_n , but levels off for high E_n . In sharp contrast, $\langle\Delta E_R\rangle$ decreases with E_n . The variation of $-\langle\Delta E\rangle$ with E_n , as well as the opposite trend between the CET and RET efficiencies, suggest different mechanism for low- and high- E_n collisions. This is consistent with the approach of Dashevskaya *et al.*,¹² in which collisions are divided into direct (single-encounter) and chattering (multiple-encounter) collisions. The differences between these two types of collisions are discussed further below.

Fig. 5 shows the average total ($-\langle\Delta E\rangle$) and rotational ($\langle\Delta E_R\rangle$) energy transfer per collision as functions of E_n , as E' is varied. Again, each data point represents a different trajectory subset, where each subset has a different E_n value. Increasing the initial excitation of propane transfers more energy at each encounter to the argon bath gas, in agreement with the results of our earlier work.⁴ The resultant higher speed of argon reduces the probability of further atom–atom encounters and lowers the total number of encounters for systems with higher E' . Similar variations with initial excitation energy are observed for Ne and He systems.

C. Rotational and total energy transfer mechanism

Fig. 6 plots the internal, $-\langle\Delta E\rangle_l$, and rotational, $\langle\Delta E_R\rangle_l$, energy transferred during the l th encounter, for the trajectory subsets with total encounter number $E_n = 1 - 8$, for propane + argon at $E' = 15000 \text{ cm}^{-1}$. Note that at fixed E_n , the energy transfer per collision is the sum of the energy transfer per encounter for each subset with encounter number E_n , and averaged over the trajectory subsets:

$$\langle\Delta E\rangle = \frac{\sum_{E_n=1}^{\infty} N(E_n) \sum_{l=1}^{E_n} \langle\Delta E\rangle_l}{\sum_{E_n=1}^{\infty} N(E_n)} \quad (7)$$

For collisions with only one atom–atom encounter ($E_n = 1$), there is an energy flow from propane to argon

$$-\langle\Delta E\rangle_{l=1} > 0$$

accompanied by a large increase in the rotational energy

$$\langle\Delta E_R\rangle_{l=1} > 0$$

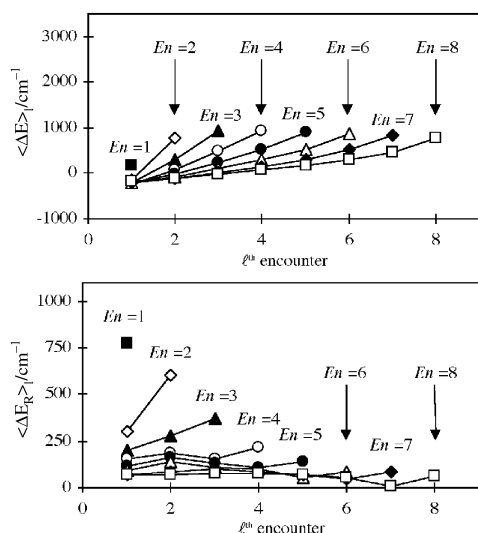


Fig. 6 Propane + argon internal, $-\langle \Delta E \rangle_l$, and rotational, $\langle \Delta E_R \rangle_l$, energy transferred per encounter during the l th encounter, for the trajectory subsets with total encounter number $En = 1-8$, at $E' = 15000 \text{ cm}^{-1}$.

In contrast, for collisions with $En > 1$, initially energy flows from argon to propane, but flows from propane to argon in subsequent encounters. In general, the magnitude of $-\langle \Delta E \rangle_l$ decreases with En . For the trajectory subsets with $En \leq 4$, $\langle \Delta E_R \rangle_l$ increases with l but remains smaller than for impulsive collisions with $En = 1$. For $En \geq 4$, $\langle \Delta E_R \rangle_l$ remains roughly constant and even decreases slightly at high l . Hence for high En the lower efficiency of the RET pathway results in $\langle \Delta E_R \rangle$ which decreases with En (Fig. 3 and 5).

The key to understanding these mechanisms lies in the variation of CET and RET with impact parameter, b . The circles in Fig. 1 show schematically where the centre of the incoming monatomic collider might impact on the propane molecule at varying impact parameters $b = 0.1-0.5 \text{ nm}$. (The actual location of initial impact will depend on the relative orientations of the colliders.) The opacity function (probability of an inelastic collision) is unity for $b < ca. 0.4 \text{ nm}$, resulting in "head-on" collisions. For $ca. 0.4 \text{ nm} < b < ca. 0.6 \text{ nm}$, the opacity function is decreasing and any resultant collisions tend to be "glancing" collisions. For $b > ca. 0.6 \text{ nm}$, the opacity function decreases to zero.

Fig. 7 plots the normalised distribution of propane + Ar trajectories in each subset with encounter number, En , and impact parameter, b , within the specified range, for $E' = 15000$

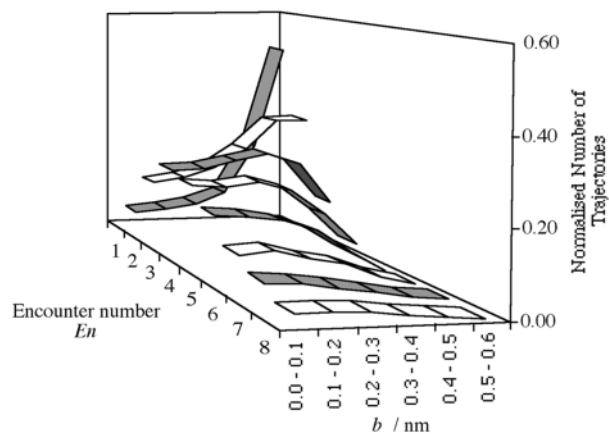


Fig. 7 Normalised distribution of propane + Ar trajectories in each subset with encounter number, En , and impact parameter, b , within the specified range, for $E' = 15000 \text{ cm}^{-1}$.

cm^{-1} (cf. our earlier work¹³). Trajectories are in bins of impact parameter with a width of 0.1 nm .

Single-encounter ($En = 1$) and double-encounter ($En = 2$) collisions are predominantly glancing collisions with a smaller, but significant, number of head-on collisions. These glancing collisions must involve the argon atom impacting a methyl hydrogen at the ends of the propane substrate (Fig. 1), producing high torque and large rotational ($T \rightarrow R$) energy transfer and moderate total ($V \rightarrow T$) energy transfer from propane to argon (Fig. 4-6).

Trajectories with $En = 3-6$ are dominated by head-on collisions. The torque of the initial encounter is lessened since b is smaller and results in lower rotational ($T \rightarrow R$) energy transfer than single- and double-encounter collisions. These head-on collisions result in ($T \rightarrow V$) energy transfer from argon to propane in the first encounter (Fig. 4-6). Subsequent encounters produce more torque with slightly increased rotational energy transfer (Fig. 6). Since the first encounter(s) has (have) significantly reduced the collider relative velocities, the energy flow is reversed in later encounters with net $V \rightarrow T$ energy transfer from the hot propane vibrations into the cold translational degree of freedom. There are very few trajectories with large En encounter numbers (Fig. 2, 3, and 7), but these continue the trend of lower rotational ($\langle \Delta E_R \rangle$) energy transfer and greater total ($-\langle \Delta E \rangle$) energy transfer.

Head-on collisions tend to have longer collision duration (as measured by En), lower rotational energy transfer and greater total energy transfer, while glancing collisions tend to have shorter collision duration, higher rotational energy transfer and lower total energy transfer.

The temporal behaviour of propane + neon and propane + helium systems are qualitatively similar to that of propane + argon. For example, Fig. 8 displays propane + helium data analogous to the propane + argon data of Fig. 6. The reduced rotational ($\langle \Delta E_R \rangle$) energy transfer and significant increase in total ($-\langle \Delta E \rangle$) energy transfer for helium bath gas,^{3,4} compared to neon and argon bath gases (Fig. 4, 6 and 8), can be attributed to the light mass of the helium collider. All other things being equal, the impulse in a single propane + monatomic encounter will be comparable for the three bath gases, resulting in comparable changes in relative momentum. However, this results in a much larger change in kinetic energy for small reduced mass than for large reduced mass, which

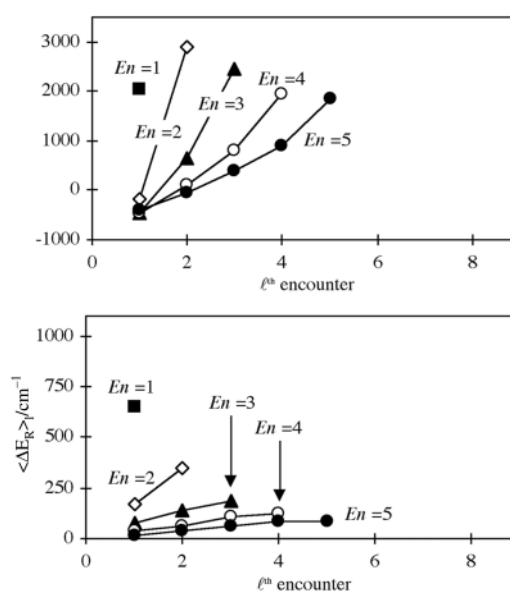


Fig. 8 Propane + helium internal, $-\langle \Delta E \rangle_l$, and rotational, $\langle \Delta E_R \rangle_l$, energy transferred per encounter during the l th encounter, for the trajectory subsets with total encounter number $En = 1-5$, at $E' = 15000 \text{ cm}^{-1}$.

explains the much enhanced total ($V \rightarrow T$) energy transfer from propane to helium. The smaller mass of helium also results in reduced torque during an encounter, compared to neon and argon, explaining the relative magnitudes of rotational ($T \rightarrow R$) energy transfer.

D. Temporal evolution of the energy distribution

To further examine the temporal behaviour we consider the time-evolution of the energy distribution $B(E, J, E', J', l)$ during the course of the collision. Analysis of the $B(E, E_R, E', E_R', l)$ distribution^{14,34} can be applied to each of the $\{En\}$ subsets of trajectories allowing the monitoring of the propane (internal) energy:

$$\bar{B}_{En}(E, E', l) = \int_0^\infty B_{En}(E, E_R, E', E_R', l) dE_R \quad (8)$$

$\bar{B}_{En}(E, E', l)$ (eqn. (8) and Fig. 9), for propane + argon at $E' = 15\,000\text{ cm}^{-1}$, restricted to $En = 3$ and $En = 5$, which has an initial near-microcanonical distribution, becomes more dispersed with each encounter. \bar{B}_{En} is biased towards negative ΔE values giving net $V \rightarrow T$ energy flow. At higher values of l , B_{En} is much more dispersed.

A change of variables to using the approximate relationship eqn. (5), allows the monitoring of the evolution of the propane rotational energy:

$$\bar{B}_{En}(E_R, E_R', l) = \int_0^\infty B_{En}(E, E_R, E', E_R', l) dE \quad (9)$$

The rotational energy distribution (eqn. (9) and Fig. 10), which has an initial Boltzmann distribution, shows similar dispersion behaviour. In this case, $\bar{B}_{En}(E_R, E_R', l)$ is biased to positive values which corresponds to net $V, T \rightarrow R$ energy flow. The conservation of angular momentum restricts the amount of this energy flow leading to smaller dispersion.

Fig. 11 plots $P_{En}(E, E')$ and $P_{En}(E_R, E_R')$ (i.e. the final \bar{B}_{En} distributions: eqn. (2)) for $En = 1-5$ averaged over all inelastic collisions. Although the individual energy transfers *per encounter*, $-\langle \Delta E \rangle_l$ (Fig. 2 and 8), are *slightly* smaller for larger

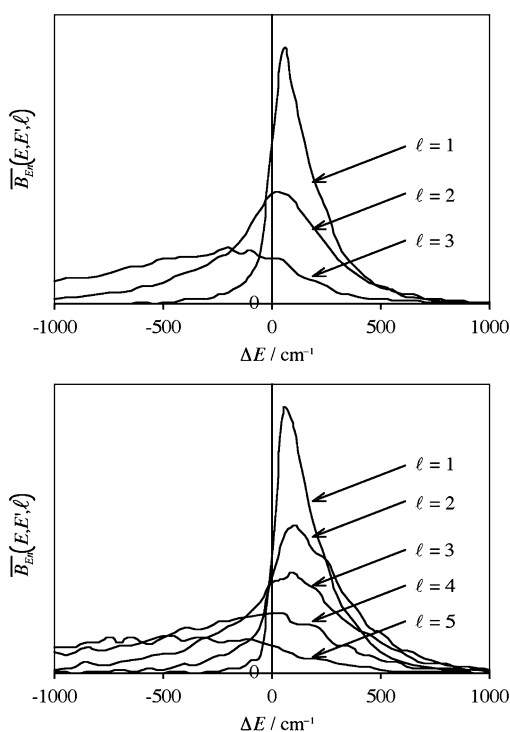


Fig. 9 $\bar{B}_{En}(E, E', l)$ for propane + argon systems at $E' = 15\,000\text{ cm}^{-1}$, with $1 \leq l \leq En$ for $En = 3$ and 5 .

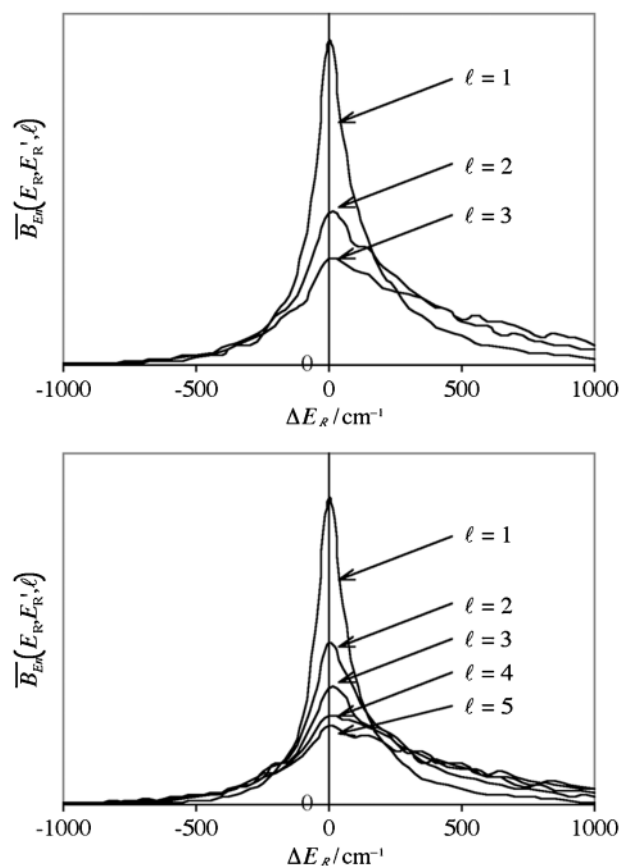


Fig. 10 $\bar{B}_{En}(E_R, E_R', l)$ for propane + argon systems at $E' = 15\,000\text{ cm}^{-1}$, with $1 \leq l \leq En$ for $En = 3$ and 5 .

En than at smaller En , the larger number of encounters results in larger $-\langle \Delta E \rangle$ (Fig. 5) at larger En : $P_{En}(E, E')$ is more biased to negative ΔE . In contrast, $P_{En}(E_R, E_R')$ remains more sharply peaked at all En than $P_{En}(E, E')$.

These results are reminiscent of diffusive models of CET and RET, where the flow of energy between the substrate's internal motions and the intermolecular relative motions is described by stochastic Smoluchowski-type equations.^{12,14-16,45} In the current calculations, the equations of motion are chaotic, resulting in quasi-random atom-atom encounters and quasi-random energy flow during the collision.

E. Considerations of qualitative versus quantitative predictions

The results of the current work are qualitative, not quantitative. Comparison of HS results and those of full quasiclassical trajectory simulations have been made in a previous paper.⁴ The HS model predicts CET and RET values that are higher than trajectories using pairwise-additive Lennard-Jones and atom pairwise-additive Buckingham-exponential intermolecular potentials.⁴ This is consistent with numerous works which concluded that CET depends mainly on the repulsive part of the intermolecular potential and that, in general, a harder repulsive part results in larger energy transfers (see for example ref. 23,24,46).

We have not attempted to compare the calculated values of the present work with experimental determinations of $\langle \Delta E \rangle$ for propane systems because to the best of our knowledge, there has been no experimental study of CET in propane + rare gas systems. "Indirect" studies of related systems (e.g., 2-bromopropane + neon⁴⁷ and deuterated cyclopropane + helium⁴⁸) did not directly measure CET quantities, but inferred them from pressure-dependent thermal reaction rates at elevated temperatures. These and some more recent studies using time-

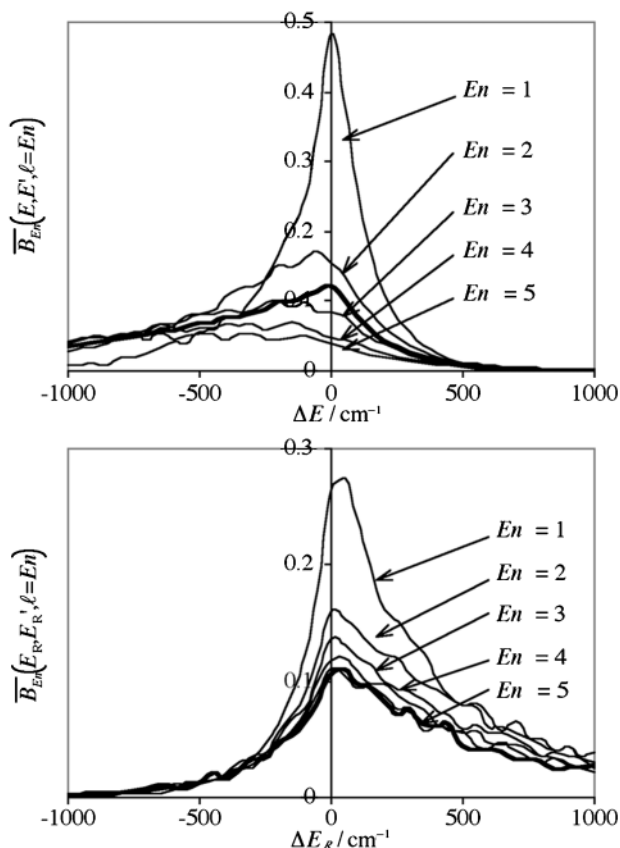


Fig. 11 $P_{En}(E, E') = \bar{B}_{En}(E, E', l=En)$ and $P_{En}(E_R, E_R') = \bar{B}_{En}(E, E', l=En)$ for propane + argon systems at $E' = 15000 \text{ cm}^{-1}$. The total (ΔE) and rotational (ΔE_R) energy transfer distributions, $P(E, E')$ and $P(E_R, E_R')$ respectively, are indicated by the thick lines. The $En = 5$ for $P_{En}(E_R, E_R') = \bar{B}_{En}(E, E', l=En)$ curve lies under the thick $P(E_R, E_R')$ curve.

resolved optoacoustic spectroscopy (e.g., $\text{C}_3\text{F}_8 + \text{argon}$)²⁶ reveal no information about RET. Furthermore, the experiments involved fitting CET parameters to observed data using one-dimensional functional forms of $P(E, E')$.¹⁰ Our previous,⁴ and present calculations clearly show the two-dimensional dependence of the energy transfer probability kernel $P(E, E', J, J')$ on both the internal energy E and the rotational state J , indicating that the original experiments should be re-examined using two-dimensional forms for $P(E, E', J, J')$.

IV. Summary and conclusions

Trajectory calculations of propane + rare gas systems have been performed using HS intermolecular potentials. Inelastic collisions are classified by the total number (En) of atom–atom encounters, which is a measure of the collision duration. En is dependent on the reduced mass of the system, being largest for argon collider and smallest for helium.

CET increases with En but saturates for large En . In contrast, RET decreases with En (Fig. 3 and 5). Detailed analysis of the temporal behaviour (Fig. 6 and 8–11) found that direct collisions with small En transfer large amount of internal and rotational energy per encounter, whereas the energy transfer per encounter is smaller for large En . This is consistent with the CET models of Dashevskaya *et al.*¹² that investigated the differences between direct (one encounter) collisions and chattering (multiple encounter) collisions.

CET and RET depend on the impact parameter b . In general, small b results in a large number of encounters,¹³ but inefficient CET and RET per encounter. On the other hand, large b results in a smaller number of encounters,¹³ but more

efficient total energy transfer. The dependence is due to the shape of the molecule and is especially important for large polyatomic substrates. This is very significant since many workers believed that RET (and hence CET) depends on the shape of polyatomics, being more efficient for prolate top molecules such as propane and ethane than for spherical top molecule such as methane. This reinforces the notion that the “one-dimensional” master equation treatment of CET must be generalised to include RET as well as the shape of the polyatomics.

Previous trajectory studies by our group and others have found that there is a strong correlation between the steepness of the repulsive interaction and the predicted CET,^{16,23,24,28,46} implying that the present model would overestimate CET, but provide good qualitative trends for CET.

To the best of our knowledge, there has been no experimental study of CET in propane + rare gas systems. Moreover, experiments on related systems involved fitting CET parameters to rate data using one-dimensional functional forms of $P(E, E')$.¹⁰ Our calculations clearly indicate that these experiments should be re-examined using two-dimensional forms for $P(E, E', J, J')$, which depend on both the internal energy E and the rotational state J .

The multiple direct encounter model of the present work, has presented information about the CET mechanism of propane + rare gas systems, which are difficult to access via more traditional QCT simulations, because the simplified dynamics allow more numerical experiments to be performed with the same computer resources.

Acknowledgements

The support of an Australian Research Council Large Grant and the Australian National University Supercomputer Facility are gratefully acknowledged. KFL thanks Ms Jeanne Lee (李静宁) for encouraging and helpful discussions.

References

- 1 R. G. Gilbert and S. C. Smith, *Theory of Unimolecular and Recombination Reactions*, Blackwell Scientific, Oxford, 1990.
- 2 I. Oref and D. C. Tardy, *Chem. Rev.*, 1990, **90**, 1407.
- 3 A. Linhananta and K. F. Lim, *Phys. Chem. Chem. Phys.*, 1999, **1**, 3467.
- 4 A. Linhananta and K. F. Lim, *Phys. Chem. Chem. Phys.*, 2000, **2**, 1385.
- 5 U. Grigoleit, T. Lenzer, K. Luther, M. Mützel and A. Takahara, *Phys. Chem. Chem. Phys.*, 2001, **3**, 2191.
- 6 (a) H. Hippler, H. W. Schranz and J. Troe, *J. Phys. Chem.*, 1986, **90**, 6158; (b) H. W. Schranz and J. Troe, *J. Phys. Chem.*, 1986, **90**, 6168.
- 7 I. Koifman, E. I. Dashevskaya, E. E. Nikitin and J. Troe, *J. Phys. Chem.*, 1995, **99**, 15348.
- 8 J. Troe, *J. Chem. Phys.*, 1977, **66**, 4745.
- 9 (a) S. C. Smith and R. G. Gilbert, *Int. J. Chem. Kinet.*, 1988, **20**, 307; (b) S. C. Smith and R. G. Gilbert, *Int. J. Chem. Kinet.*, 1988, **20**, 979.
- 10 D. C. Tardy and B. S. Rabinovitch, *Chem. Rev.*, 1977, **77**, 369.
- 11 (a) M. Liu, S. Nordholm, G. Nyman and J. Davidsson, *Chem. Phys. Lett.*, 1993, **211**, 189; (b) M. Liu, T. D. Sewell and S. Nordholm, *Chem. Phys.*, 1995, **199**, 83; (c) S. Nordholm and H. W. Schranz, in *Advances in Chemical Kinetics and Dynamics: Vibrational Energy Transfer Involving Large and Small Molecules*, ed. J. R. Barker, JAI Press, Greenwich, CT, 1995, vol. 2A, pp. 245–281. (d) M. Liu, J. Davidsson and S. Nordholm, *Chem. Phys.*, 1995, **201**, 121; (e) L. E. B. Börjesson, M. Liu and S. Nordholm, *Chem. Phys.*, 1997, **221**, 253; (f) S. Nordholm, L. E. B. Börjesson, M. Liu and H. Svedung, *Ber. Bunsen-Ges. Phys. Chem.*, 1997, **101**, 574; (g) H. Svedung, L. E. B. Börjesson, N. Markovic and S. Nordholm, *Chem. Phys.*, 1998, **236**, 189; (h) H. Svedung, N. Markovic and S. Nordholm, *Chem. Phys.*, 1999, **248**, 195.

- 12 (a) E. I. Dashevskaya, E. E. Nikitin and I. Oref, *J. Phys. Chem.*, 1993, **97**, 9397; (b) E. I. Dashevskaya, E. E. Nikitin and I. Oref, *J. Phys. Chem.*, 1995, **99**, 10797.
- 13 V. Bernshstein, K. F. Lim and I. Oref, *J. Phys. Chem.*, 1995, **99**, 4531.
- 14 K. F. Lim and R. G. Gilbert, *J. Chem. Phys.*, 1986, **84**, 6129.
- 15 K. F. Lim and R. G. Gilbert, *J. Chem. Phys.*, 1990, **92**, 1819.
- 16 K. F. Lim and R. G. Gilbert, *J. Phys. Chem.*, 1990, **94**, 77.
- 17 W. L. Hase, K. F. Lim, Program MARINER: A general Monte Carlo classical trajectory computer program (1999 version), 1990. Program is available from second author, Centre for Chiral and Molecular Technologies, Deakin University, Geelong, VIC 3217, Australia <http://www.deakin.edu.au/~lim/>.
- 18 W. L. Hase, R. J. Duchovic, X. Hu, A. Komornicki, K. F. Lim, D.-H. Lu, G. H. Peslherbe, K. N. Swamy, S. R. Van de Linde, A. Varandas, H. Wang and R. J. Wolf, *Quantum Chem. Program Exchange Bull.*, 1996, **14**(4), 43 [Supplementary material: QCPE Program 671, a 13,435-line Fortran program] <http://qcpe.chem.indiana.edu/>.
- 19 H. J. Lindner, *Tetrahedron*, 1974, **30**, 1127.
- 20 R. T. Morrison and R. N. Boyd, *Organic Chemistry*, Simon and Schuster, Newton, MA, 5th edn., 1987.
- 21 J. E. Huheey, *Inorganic Chemistry*, Harper and Row, New York, 3rd edn., 1983.
- 22 R. N. Porter and L. M. Raff, in *Dynamics of Molecular Collisions*, ed. W. H. Miller, Plenum Press, New York, 1976, vol. B, p. 1.
- 23 K. F. Lim, *J. Chem. Phys.*, 1994, **100**, 7385.
- 24 K. F. Lim, *J. Chem. Phys.*, 1994, **101**, 8756.
- 25 (a) D. C. Tardy, *J. Phys. Chem.*, 1993, **97**, 5624; (b) D. C. Tardy, *J. Chem. Phys.*, 1993, **99**, 963; (c) K. M. Beck, R. J. Gordon and D. C. Tardy, in *Advances in Chemical Kinetics and Dynamics: Vibrational Energy Transfer Involving Large and Small Molecules*, ed. J. R. Barker, JAI Press, Greenwich, CT, 1995, vol. 2B, pp. 299–332; (d) H. Hippler, J. Troe and H. J. Wendelken, *J. Chem. Phys.*, 1983, **78**, 6718; (e) H. Hippler, L. Lindemann and J. Troe, *J. Chem. Phys.*, 1985, **83**, 3906; (f) B. M. Toselli, J. D. Brenner, M. L. Yerram, W. E. Chin, K. D. King and J. R. Barker, *J. Chem. Phys.*, 1991, **95**, 176; (g) B. M. Toselli and J. R. Barker, *J. Chem. Phys.*, 1992, **97**, 1809.
- 26 D. C. Tardy and B. H. Song, *J. Phys. Chem.*, 1993, **97**, 5628.
- 27 H. Hippler, J. Troe and H. J. Wendelken, *J. Chem. Phys.*, 1983, **78**, 6709.
- 28 T. Lenzer, K. Luther, J. Troe, R. G. Gilbert and K. F. Lim, *J. Chem. Phys.*, 1995, **103**, 626.
- 29 (a) B. J. Alder and T. E. Wainwright, *J. Chem. Phys.*, 1959, **31**, 459; (b) M. P. Allen and D. J. Tildesley, *Computer Simulations of Liquids*, Oxford Science Publications, Oxford, 1990; (c) J. M. Haile, *Molecular Dynamics Simulation: Elementary Methods*, Wiley, New York, 1992.
- 30 (a) J. M. Bowman, B. Gazdy and Q. Sun, *J. Chem. Phys.*, 1989, **91**, 2859; (b) W. H. Miller, W. L. Hase and C. L. Darling, *J. Chem. Phys.*, 1989, **91**, 2863; (c) G. H. Peslherbe and W. L. Hase, *J. Chem. Phys.*, 1994, **100**, 1179; (d) K. F. Lim and D. A. McCormack, *J. Chem. Phys.*, 1995, **102**, 1705; (e) D. A. McCormack and K. F. Lim, *J. Chem. Phys.*, 1995, **103**, 1991; (f) G. H. Peslherbe and W. L. Hase, *J. Chem. Phys.*, 1996, **104**, 9445; (g) D. Shen and H. O. Pritchard, *J. Chem. Soc., Faraday Trans.*, 1996, **92**, 4357; (h) D. A. McCormack and K. F. Lim, *J. Chem. Phys.*, 1997, **106**, 572; (i) D. A. McCormack and K. F. Lim, *Phys. Chem. Chem. Phys.*, 1999, **1**, 1.
- 31 (a) S. Bosanac, *Phys. Rev. A*, 1980, **22**, 2617; (b) R. J. Marsh and A. J. McCaffery, *Chem. Phys. Lett.*, 2001, **335**, 134.
- 32 P. G. Mezey, in *Reviews in Computational Chemistry*, ed. K. B. Lipkowitz and D. B. Boyd, VCH, New York, 1990, vol. 1, pp. 265–294.
- 33 (a) N. B. Slater, *Proc. Camb. Phil. Soc.*, 1939, **35**, 56; (b) N. B. Slater, *Theory of Unimolecular Reactions*, Cornell University Press, Ithaca, NY, 1959.
- 34 K. F. Lim and R. G. Gilbert, *J. Phys. Chem.*, 1990, **94**, 72.
- 35 (a) B. Efron, *SIAM Rev.*, 1979, **21**, 460; (b) P. Diaconis and B. Efron, *Sci. Am.*, 1983, **248**(5), 96–108.
- 36 K. F. Lim, Program PEERAN: $P(E,E')$ error analysis program (2001 version). Program is available from author, Centre for Chiral and Molecular Technologies, Deakin University, Geelong, VIC 3217, Australia <http://www.deakin.edu.au/~lim/>.
- 37 D. A. McQuarrie, *Statistical Mechanics*, Harper and Row, New York, 1976.
- 38 A. J. Stone, *The Theory of Intermolecular Forces*, Oxford University Press, Oxford, 1996.
- 39 K. F. Lim, *Quantum Chem. Program Exchange Bull.*, 1994, **14**(1), 3 [supplementary material: QCPE Program 643, a 549-line Fortran program] <http://qcpe.chem.indiana.edu/>.
- 40 G. Lendvay and G. C. Schatz, *J. Phys. Chem.*, 1992, **96**, 3752.
- 41 (a) E. F. Greene and A. Kuppermann, *J. Chem. Educ.*, 1968, **45**, 361; (b) J. I. Steinfeld, J. S. Francisco and W. L. Hase, *Chemical Kinetics and Dynamics*, Prentice Hall, Upper Saddle River, NJ, 2nd edn., 1999.
- 42 W. D. Lawrance and A. E. W. Knight, *J. Chem. Phys.*, 1983, **79**, 6030.
- 43 (a) J. Troe, *J. Phys. Chem.*, 1979, **83**, 114; (b) J. Troe, *J. Chem. Phys.*, 1977, **66**, 4758; (c) J. Troe, *Ber. Bunsen-Ges. Phys. Chem.*, 1983, **87**, 161; (d) R. G. Gilbert, K. Luther and J. Troe, *Ber. Bunsen-Ges. Phys. Chem.*, 1983, **87**, 169.
- 44 (a) M. J. T. Jordan, K. C. Thompson and M. A. Collins, *J. Chem. Phys.*, 1995, **102**, 5647; (b) K. C. Thompson, M. J. T. Jordan and M. A. Collins, *J. Chem. Phys.*, 1998, 8302; (c) R. P. A. Bettens and M. A. Collins, *J. Chem. Phys.*, 1999, **111**, 816; (d) D. H. Zhang, M. A. Collins and S.-Y. Lee, *Science*, 2000, **290**(5493), 961–963.
- 45 E. I. Dashevskaya, I. Litvin, E. E. Nikitin, I. Oref and J. Troe, *Phys. Chem. Chem. Phys.*, 2000, **2**, 2251.
- 46 M. Bruehl and G. C. Schatz, *J. Phys. Chem.*, 1988, **92**, 7223.
- 47 T. C. Brown, K. D. King and R. G. Gilbert, *Int. J. Chem. Kinet.*, 1987, **19**, 851.
- 48 V. V. Krongauz and B. S. Rabinovitch, *J. Chem. Phys.*, 1983, **78**, 3872.